



## A Nonlinear Error Compensator for FDM 3D Printed Part Dimensions Using a Hybrid Algorithm Based on GMDH Neural Network

Hamid Haghshenas Gorgani<sup>1, \*</sup>, Hossein Korani<sup>2</sup>, Reihaneh Jahedan<sup>3</sup> and Sharif Shabani<sup>4</sup>

<sup>1</sup>Engineering Graphics Center, Sharif University of Technology, Tehran, Iran

<sup>2</sup>School of Mechanical Engineering, College of Engineering, University of Tehran, Tehran, Iran

<sup>3</sup>Mechanical Science & Engineering, Grainger College of Engineering, University of Illinois at Urbana Champaign, USA

<sup>4</sup>Mechanical Engineering Department, Sharif University of Technology, Tehran, Iran

### Abstract

Following the advances in Computer-Aided Design (CAD) and Additive Manufacturing (AM), with regards to the numerous benefits of the Fused Deposition Modeling (FDM) as a popular AM process, resolving its weaknesses has become increasingly important. A serious problem of the FDM is the dimensional error or size difference between the CAD model and the actual 3D printed part. In this study, the approach is compensating the error regardless of its source. At First, all parameters affecting the dimensional accuracy of FDM are comprehensively identified. Then, multi-input–single-output (MISO) data is prepared by designing experiments using the Taguchi method and obtaining the results from 3D printed samples. Next, a GMDH neural network is applied, which uses a simple nonlinear regression formula in each neuron but can create very complex neuron combinations. So, it is possible to analyze small or even noisy data. Regulatory parameters of the Neural Net have been optimized to increase efficiency. The case study shows a decrease in the RSME for the Nominal CAD Model from 0.377 to 0.033, displaying the compensator's efficiency.

**Keywords:** Additive Manufacturing, Fused Deposition Method, Error Compensation Model, GMDH Neural Network.

### Introduction

Rapid Prototyping (RP) is a technology that makes transforming digital designs into solid models possible. It can be used to produce machine parts, prototypes, and molds [1]. Over the last decades, advances have been made in Computer-Aided Design (CAD) and RP. This has given designers the chance to generate a concept faster and more freely [2]. RP is usually used to produce parts by Additive Manufacturing (AM) technologies. In AM, layers of material are gradually added to form the required shape. This is contrary to conventional manufacturing techniques, e.g., forming or material removal [3]. Numerous AM processes are available including Stereolithography (SLA), Laminated Object Manufacturing (LOM), Selective Laser Sintering (SLS), Fused Deposition Modeling (FDM) and etc. [1].

FDM is an AM process in which semi-molten plastic material is extruded from a nozzle. In this process, thin layers of plastic form a solid shape from bottom to top [4]. Normally, a filament of the material is fed into a heated nozzle with a roller mechanism. A thin layer of the material is extruded out of the nozzle, forming the layer by moving the nozzle in the x-y plane. This happens over a build surface that is capable of moving vertically in the z-axis direction. Different materials are used in this process, when the most common is Acrylonitrile Butadiene

\* Corresponding Author. Tel: +98-21-66164823, E-Mail: [h\\_haghshenas@sharif.edu](mailto:h_haghshenas@sharif.edu)

Styrene (ABS) [5]. Several advantages of this process such as simplicity, low price, and durability of produced parts are the most important reasons that FDM can be used to manufacturing the functional parts, apart from the prototypes. However, FDM has many drawbacks of its own [6]. Many research projects have been carried out to optimize process parameters and minimize the drawbacks, including low strength, rough surface finish, long build time and poor dimensional accuracy [7]. So, one of the most important challenges in FDM is dimensional accuracy, i.e., the difference between the manufactured model with the presented CAD file.

Numerous research papers have discussed the accuracy of parts printed with FDM machines, most of which considering shrinkage as the most important cause. Sood *et al.* (2009) used Taguchi's design to run 27 experiments. They came out with optimum values for their parameters [6]. El-Katatny *et al.* [8] investigated the dimensional errors of FDM printed anatomical replicas derived from computed tomography (CT). They showed that the replicas are generally smaller than the actual size. Percoco *et al.* [9] used three process parameters, i.e. air gap, temperature and size. They aimed to investigate the deviations in holes and shafts in order to improve the mating process in assembly. Mohamed *et al.* [10] used second-order Definitive Screening Design (DSD) and Artificial Neural Network (ANN) to optimize six process parameters of printing cylindrical samples. Akbas *et al.* [11] carried out experimental and numerical experiments in order to find the effects of material, feed rate, nozzle temperature and height on dimensional accuracy of an FDM printed strip. Park *et al.* [12] compared FDM with other AM techniques to produce dental casts. They concluded that FDM is the inferior method in terms of dimensional accuracy. Peng *et al.* [13] optimized process parameters to print a confirmation experiment. The final part improved in dimensional accuracy; however, its build time increased. Mendricky *et al.* [14] investigated the effect of multiple process parameters on dimensional accuracy, surface roughness, material consumption, and build time. They concluded that layer height is the most important factor affecting dimensional accuracy and surface roughness. Chohan *et al.* [15] optimized vapor smoothing process parameters to gain improved surface finishing and dimensional accuracy in biomedical applications. Garg *et al.* [16] also studied the accuracy of ABS samples after cold vapor smoothing with acetone. Nsengimana *et al.* [17] compared different post-processing techniques in FDM and SLA, concluding that an acetone bath on FDM printed ABS samples has the best result. Garg *et al.* [18] used FDM to produce mold samples and achieved acceptable results.

Many researchers proposed a compensation model to produce more accurate parts. Tong *et al.* [19] extended the approach of software error compensation. They used this to reduce errors in FDM and SLA parts. Li *et al.* [20] studied a printing error compensator to print electronic parts with connecting brackets. Pacurar *et al.* [21] used FEM to predict printed sample dimensions. They developed a software application to calculate the original CAD parameters using linear regression. Yaman [22] proposed a novel approach in which "shrinkage itself is utilized to eliminate the effects of shrinkage." In this method, inside lines are designed over the perimeter of holes to prevent them from decreasing their size. He also developed numerical shrinkage models, which were mostly in agreement with experimental data. Dilberoglu *et al.* [23] expanded Yaman's approach and confirmed his findings by running more experiments and predicting FEA models. Their approach can only be used to compensate holes and slots dimensions. Noriega *et al.* [24] developed a model to predict the dimensions of the manufactured parts and determine the CAD model dimensions using ANN and an optimization algorithm. However, they only used a limited number of process parameters in a particular condition. Therefore, the performed researches fall into the framework of two basic approaches: error avoidance approach by reduction of its sources and error compensation approach, regardless of the sources [25]. A comparison of the two approaches shows that most of the

research can be categorized within the first approach which focuses on building more accurate samples by using different materials and optimizing the process parameters [26]. However, these methods are less frequently used due to technical problems and high implementing costs. In contrast, the second method is more practical because of its general attitude and the lack of need for extensive changes in methods and parameters. However, the presented models are mostly limited to specific geometries and invalid in other ones. Furthermore, reviewing the studies on second approach shows that each of them addressed a limited number of FDM process parameters (rarely reaching four or five). Another noteworthy point is that these models are based on a small number of experiments due to the high cost, greatly increasing the risk of noise in the results.

Accordingly, the main challenge of this research is to provide an error compensator that is not limited to a specific geometry, is low cost, flexible, includes most process parameters, and short data or possible noise has the least negative impact on its performance.

In this paper, first, ten process parameters are selected to study. Using Taguchi's approach, 27 experiments are carried out, and the parameters that are dominantly affecting the dimensional accuracy are found. A GMDH artificial neural network is then trained to predict the output of CAD models with respect to their process parameters. GMDH has the lowest sensitivity to short data and the adverse effects of noisy results because it uses a simple quadratic regression structure with the ability to construct complex mathematical combinations [27]. This ANN enables the determining of initial CAD dimensions in order to reach the closest dimensions to the nominal values. Finally, as a case study, a sample model is modified by the proposed compensator, then printed, and the real error reduction is evaluated.

## **Materials and Methods**

### **Parameter Identification**

Two sources have been used to identify configurable input parameters of the FDM process:

The first source is the MakerBot Replicator 2X software, which is used to receive a CAD file and pass proper information into the existing FDM machine. The parameters that can be adjusted in the software or the settings that are applied manually on the FDM machine are selected as the input parameters. A view of software setting page can be seen in Figure 1. It should be noted that this procedure will perform individually for each machine and each software.

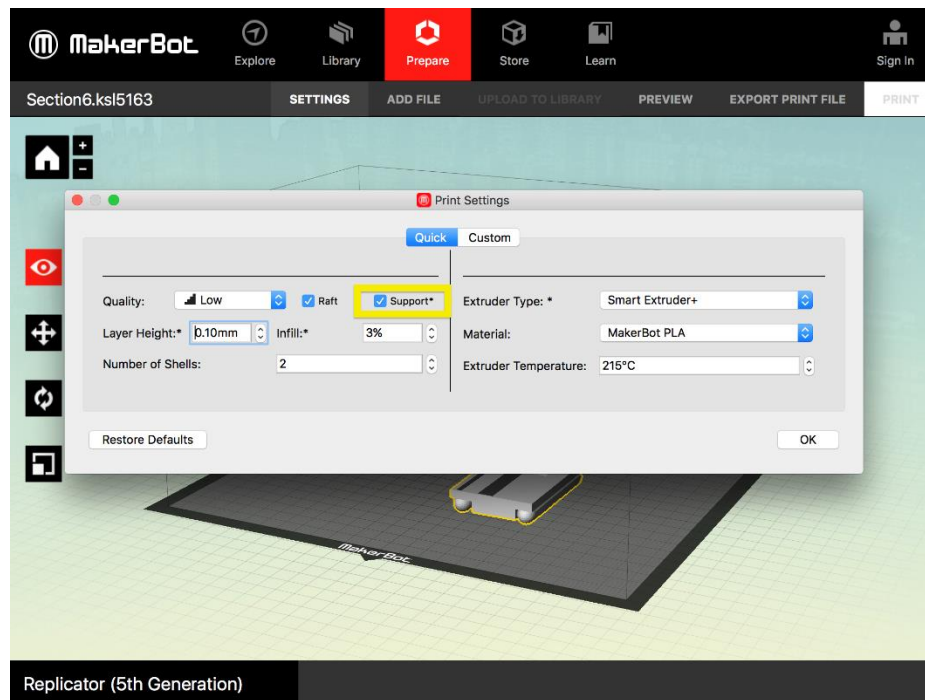


**Figure 1.** A view of Makerbot setting page

The second source is a review of the research literature on identification, optimization, or error compensation for the FDM process, particularly in recent years. It should be considered that the development of the FDM process has led to the creation of new parameters and adjustments in later software versions. Some new tools and machines did not exist in the past, so old research may have become invalidated. The results of the literature review are reported in Table 1.

**Table 1.** Literature review of input parameters of FDM process

Reference	Author(s)	Year	Input Parameters
[28]	Sood et al.	2009	Layer Thickness Air Gap Raster Angle Raster Width
[29]	Panda et al.	2009	Layer Thickness Build Orientation Air Gap Raster Angle Raster Width
[30]	Arivazhagan and Masood	2012	Build Orientation Interior Style Raster Width
[31]	Luzanin et al.	2013	Extruder Temperature

[32]	Sahu, R.K. et al.	2013	Layer Thickness Build Orientation Air Gap Raster Angle Raster Width
[33]	Bhatia, S.	2014	Print Location Build Orientation
[27]	Rayegani and Onwubolu	2014	Layer Thickness Build Orientation Air Gap Raster Angle Raster Width
[34]	Akande, S.O.	2015	Layer Thickness Infill Density
[35]	Baich, L. et al.	2015	Interior Style
[36]	Equbal, A., et al.	2017	Air Gap Raster Angle Raster Width
[37]	Narang, R. and D. Chhabra	2017	Layer Thickness Build Orientation Infill Density Interior Style No. of Shells Air Gap Raster Angle Raster Width
[38]	Qattawi, A. et al.	2017	Layer Thickness Build Orientation Infill Density Interior Style Print Speed
[39]	Aw, Y.Y., et al.	2018	Infill Density Interior Style
[40]	Deng, X., et al.	2018	Print Speed

			Layer Thickness Infill Density Extruder Temperature
[41]	Leite, M., et al.	2018	Layer Thickness Infill Density Extruder Temperature Raster Angle
[42]	Dey, A. and N. Yodo	2019	Layer Thickness Build Orientation No. of Shells Air Gap Raster Angle Raster Width Extruder Temperature
[23]	Dilberoglu et al.	2019	Print Speed Raster Width Extruder Temperature
[43]	Lyu, J. and S. Manoochehri	2019	Scale Layer Thickness Extruder Temperature Infill Density

There is an overlap of parameters between Table 1 and software settings. The ineffectiveness of some other parameters has been shown in various studies. Also, some parameters such as print speed or raster settings (Including angle and width) are not available for all printers. With regards to these points, the following eight parameters were selected as adjustable input parameters in the FDM process:

Scale, Print Location, Extruder Temperature, Angle to X-Axis (Part Orientation), Layer Thickness, Infill Density, Number of Shells, and Infill Pattern (Interior Style).

Due to the part height and warpage effects, which take the part walls out of the perpendicularity tolerance range [13], the part's height can be added to this list as the 9th parameter.

### **The Taguchi Procedure**

The conventional experimenting method of full factorial DOE is quite complex, costly, and impracticable [44, 45]. Taguchi technique minimizes the number of experiments using orthogonal arrays. In addition, it shows the effects of each independent variable (input) on the dependent variable (output) by defining a loss function with regard to the nature of the output. Next, analysis of variance (ANOVA) and signal-to-noise ratio are provided [46, 47].

As mentioned in section 2.1, nine input parameters are selected, and three levels of magnitude are considered for each parameter, as listed in Table 2. The dependent variable (output) is the error value between the part's dimensions produced by the FDM printer and the proposed CAD model. According to the nature of the output, the "smaller is better" strategy is used. The loss function is according to Equation 1 [48].

$$S/N = -10 \log \left[ \frac{1}{n} \left( \sum y^2 \right) \right] \quad (1)$$

Where  $y$  is the model dimensional error and  $n$  is the number of each experiment's replications.

**Table 2.** Input variables with their levels

No.	Variable Name	Symbol	Unit	Level 1	Level 2	Level 3
1	Scale	X1	mm	40	50	60
2	Print Location	X2	-	1:Left	2:Center	3:Right
3	Extruder Temperature	X3	C	218	230	242
4	Angle to X-Axis	X4	Degree	0	45	90
5	Layer Thickness	X5	mm	0.15	0.20	0.25
6	Infill Density	X6	%	10	20	30
7	No. of Shells	X7	-	2	3	4
8	Infill Pattern	X8	-	1: Star	2:Rectangular	3:Hexagonal
9	height	X9	mm	10	20	30

### GMDH Neural Network

The GMDH neural network is one of the best tools to solve modeling and forecasting problems for small and large amounts of data. It can even work with random or complex data structures [49]. Suppose the input is in the form of a  $\vec{X}$  vector where,  $\vec{X} = (x_1, x_2, \dots, x_n)$ , the output predicted by the neural network is  $z_i$ , and the actual output is  $y_i$ . Furthermore, assume the value of  $P$  represents the number of data pairs in the form of multi-input–single-output:

$$y_i = f(x_{i1}, x_{i2}, \dots, x_{in}), i = 1, 2, \dots, n \quad (2)$$

$$z_i = \hat{f}(x_{i1}, x_{i2}, \dots, x_{in}), i = 1, 2, \dots, n \quad (3)$$

The GMDH neural network's goal is to map the input to the actual output. To achieve this goal, it is necessary to minimize the variance between the actual output and the output predicted by the neural network. Therefore:

$$\text{Minimum} \rightarrow \sum_{i=1}^P (y_i - z_i)^2 \quad (4)$$

The predicted output is a nonlinear function in the form of Kolmogorov-Gabor polynomial:

$$z = c_0 + \sum_{i=1}^n c_i x_i + \sum_{i=1}^n \sum_{j=1}^n c_{ij} x_i x_j + \sum_{i=1}^n \sum_{j=1}^n \sum_{k=1}^n c_{ijk} x_i x_j x_k + \dots \quad (5)$$

Where  $C_i$  are polynomial coefficients and  $i, j, k \in (1, \dots, n)$ .

For the sake of simplicity, the GMDH network uses the Kolmogorov-Gabor quadratic polynomial in the following form [50]:

$$z = c_0 + c_1 x_i + c_2 x_j + c_3 x_i x_j + c_4 x_i^2 + c_5 x_j^2 \quad (6)$$

To calculate the  $C_i$  coefficients where  $i = 0, 1, \dots, 5$  regression analysis is used as follows:

$$\text{Minimize}(E) \quad , E = \frac{\sum_{i=1}^P (y_i - z_i)^2}{P} \quad (7)$$

For a set of  $P$  MISO data pairs, the above relationships can be summarized and reproduced in the following matrix form:

$$y_{P \times 1} = G \cdot C \quad (8)$$

Where:

$$y_{P \times 1} = \{y_1, y_2, \dots, y_P\}^T$$

$$C = \{c_0, c_1, c_2, c_3, c_4, c_5\}^T$$

$$G = \begin{bmatrix} 1 & x_{1u} & x_{1v} & x_{1u}x_{1v} & x_{1u}^2 & x_{1v}^2 \\ 1 & x_{2u} & x_{2v} & x_{2u}x_{2v} & x_{2u}^2 & x_{2v}^2 \\ \vdots & \vdots & \vdots & \vdots & \vdots & \vdots \\ 1 & x_{Pu} & x_{Pv} & x_{Pu}x_{Pv} & x_{Pu}^2 & x_{Pv}^2 \end{bmatrix} \quad (9)$$

To calculation of  $C$  values:

$$C = (G^T G)^{-1} G^T y \quad (10)$$

The value of  $(G^T G)^{-1} G^T$  is called the Pseudo-Inverse of the Matrix  $G$  [51-54].

At the next step, a number of neurons are chosen to compose the subsequent layer. The selection criterion is the deviation amount (error) between the predicted output and the actual output of each neuron. Let us define:

$$e_i = (y_i - z_i)^2 \quad (11)$$

For the maximum and minimum values, we have:

$$\text{Max}(e_i) = e_{max} \quad (12)$$

$$\text{Min}(e_i) = e_{min} \quad (13)$$

The critical value of error is defined as below:

$$e_c = \alpha e_{min} + (1 - \alpha) e_{max} \quad (14)$$

Where  $0 < \alpha < 1$  is called the selection pressure criterion [55]. Removable neurons are the ones in which,  $e_i > e_c$ . Obviously, selecting higher values of  $\alpha$  leads to the elimination of more

neurons.  $\alpha = 0$  means  $e_c = e_{max}$  and we will not have any exclusions. Likewise,  $\alpha=1$  means,  $e_c = e_{min}$ , and all neurons except those with the least error value will be dismissed.

Assume the maximum number of neurons allowed for each layer is  $R$ , which the user has set initially. Now, if the number of neurons remaining is greater than  $R$ , they are arranged from the lowest value of  $e_i$  to the highest. Then the first  $R$  neurons at the beginning of the list, which are the ones with the lowest  $e_i$  values, are selected to create the next layer.

It should be noted that the entire data is divided into two sets: a training set and a test set. The user determines the ratio of this division. The selection and evaluation of the quality of neurons are made on the test data set. The GMDH network training process involves adding layers, calculating regression coefficients, and removing lower quality neurons. This network is self-organizing and the output of the current layer is the input of the next layer. This process continues until at least one of the stopping conditions is met[56]. Reaching a layer with just a single neuron is the primary stopping condition. Another condition is reaching a layer whose RSME value is higher than the previous layer, which indicates that the situation is deteriorating. Furthermore, reaching the maximum number of allowed layers previously set by the user causes the operation to stop. In the latter two cases, the neuron with the best function (lowest  $e_i$ ) is selected as the output, and the other neurons in that layer are discarded.

A summary of the above steps is graphically displayed in Figure2 [57].

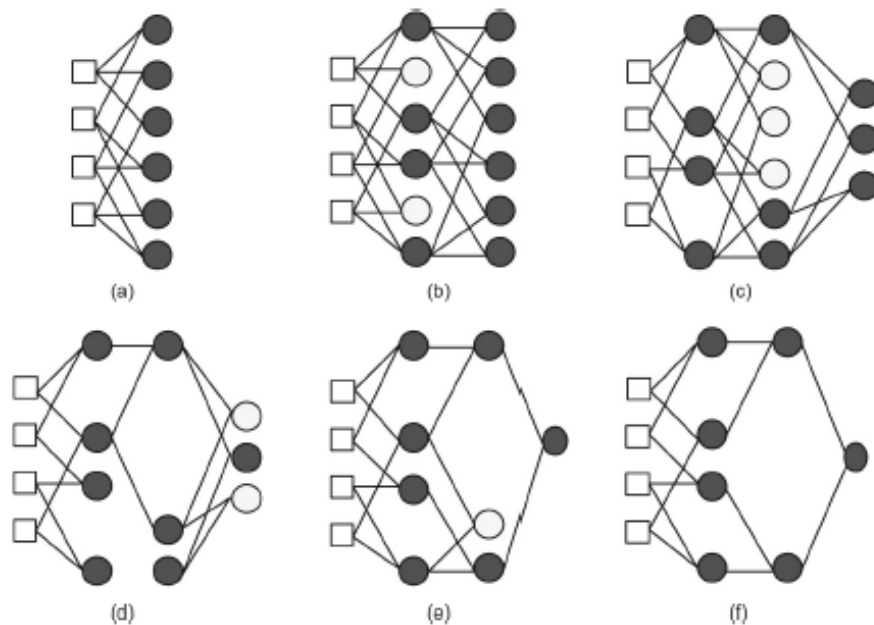


**Figure 2.** A graphical example of GMDH neural network training - (a) The first network layer with four inputs is formed. (b) After calculating the values of  $e_i$ , lower quality neurons are removed (the removed neurons are shown in white). (c) Selection of neurons in the new layer. (d) and (e), after the selection process at each stage, the network training continues until one of the stop conditions is reached. (f) The neurons which have no role in the network are removed—reconstructed from source [57]

### Compensation Model

Assume the Nominal CAD model is as shown in Figure 3, where the curve of the object's edge is arbitrary. To calculate the error of each point on the curve, first, the origin is defined; then,  $x$

and y axes are specified. It is better to choose the reference and axes with regards to the datum of the object.

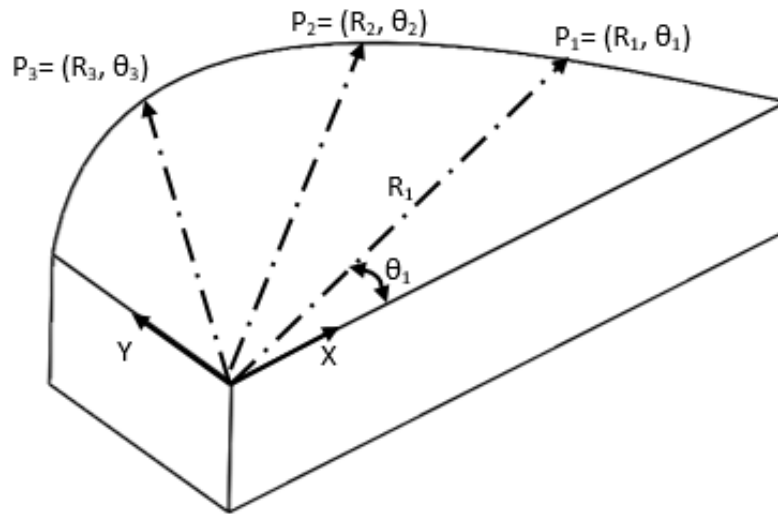


**Figure 3.** Vector Generation from Nominal CAD Model

Next, we define some points as the "exact points" on the specified curve. These points are either based on the piece's datum or such that, a good approximation of the main curve is obtained (points P1, P2, and P3 in Figure 10). Vectors that connect the coordinate system's origin to each of these points are created in the next step. For example, for the points in Figure 4, we have:

$$\vec{P}_1 = (R_1, \theta_1)$$

$$\vec{P}_2 = (R_2, \theta_2)$$

$$\vec{P}_3 = (R_3, \theta_3)$$

⋮

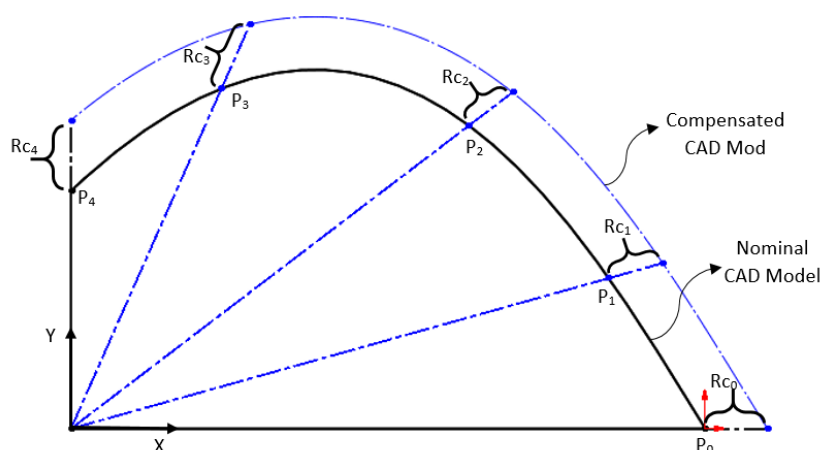


**Figure 4.** Applying Compensation on Nominal CAD Model (Generation of Compensated CAD Model).

We need nine input parameters for each point to enter information into the neural network (error compensation model). Here,  $R$  represents the scale parameter.  $\theta$  represents the angle with the  $x$ -axis. The distance of the piece from the bottom edge indicates the height parameter. Depending on the circumstances, other parameters can be set individually or in groups by adjusting the optimal value obtained from ANOVA analysis and the signal-to-noise ratio in the Taguchi algorithm.

Moving forward, these points (with nine neural network input parameters) are supplied to the optimized GMDH neural network. For each, a compensation radius value declared by  $R_{c_i}$  (where  $i = 0, 1, \dots, n$  and  $n$  is the total number of points on the curve) is taken as the neural network's output.

New points are obtained from vectors whose angles are unchanged, but their radii have increased/decreased by the value of  $R_{c_i}$ . In other words, for each point,  $R_i$  transformed to  $R_i + R_{c_i}$ . The points on the  $x$  and  $y$  axes are considered as  $P_0$  and  $P_{n+1}$ .

Afterward, the best passing spline through the points obtained from the compensated vectors is plotted as the new curve of the intended edge. The compensated CAD model is redesigned based on the implementation of this new curve to the nominal CAD model and is used for 3D printing. The compensated CAD Model of Figure 3 is presented in Figure 4.

The greater the number of points, the greater the accuracy of the fitted curve. At the same time, it will cause more complexity and consequently more computational costs and slow down the compensation process. However, due to the piecewise nature of the spline curve, it is very unlikely that the curve will go out of the smooth state by increasing the number of points, because as the number of points increases, the degree of the curve does not increase.

### The Proposed Method

In the first step, the process input parameters are identified individually and listed. Next, appropriate parameter levels are determined according to their range of application. Then, using the Taguchi method, a set of experiments is suggested. The number of experiments and consequently the amount of data obtained for neural network training may be inadequate. This is due to the uniqueness and personalization of parameters based on their application range and number of levels. In this case, a number of randomly selected points within the range of each parameter and based on the neural network needs are used as additional points, which complement the Taguchi-designed experiments. By adjusting the parameters on these points and the Taguchi method's points, the entire result is used as input data for neural network training. This data is divided into two groups: the training set and the test set. The user determines the ratio of this division ( $p$ -train), the maximum number of neurons in each layer, the maximum number of allowed layers, and the selection pressure criterion ( $\alpha$ ) by initializing the parameters. The training data with the initial configuration of GMDH network parameters is then given to the neural network, and its RSME and R-Value are determined. To optimize the neural network parametrically, experiments are once again designed by the Taguchi method for these configuration parameters ( $\alpha$ ,  $p$ -train, maximum the number of Neurons and the maximum number of layers).

The total RSME value obtained in each experiment, ANOVA analysis and  $S / N$  ratio obtained to show the amount of parameter's influence and optimal levels. Then, the GMDH neural network is trained with the training set and used as an error compensation model in the following steps.

Now, the existing Nominal CAD model, as mentioned in Section 2.4, is punctuated and gridded. For each point's polar vector, the required compensation value of  $R_{c_i}$  is obtained using the

optimized GMDH network. The compensated radius of each point is  $(R_i+R_{c_i})$  while its angle remains unchanged. Using the new radii and passing a spline, the compensated CAD model is obtained.

The 3D printing process is performed on this model and the FDM process error, which is  $R_{c_i}$  for each point, causes the printed part to have maximum compliance with the nominal CAD model.

The steps of this method can be observed in the flowchart illustrated in Figure 5.

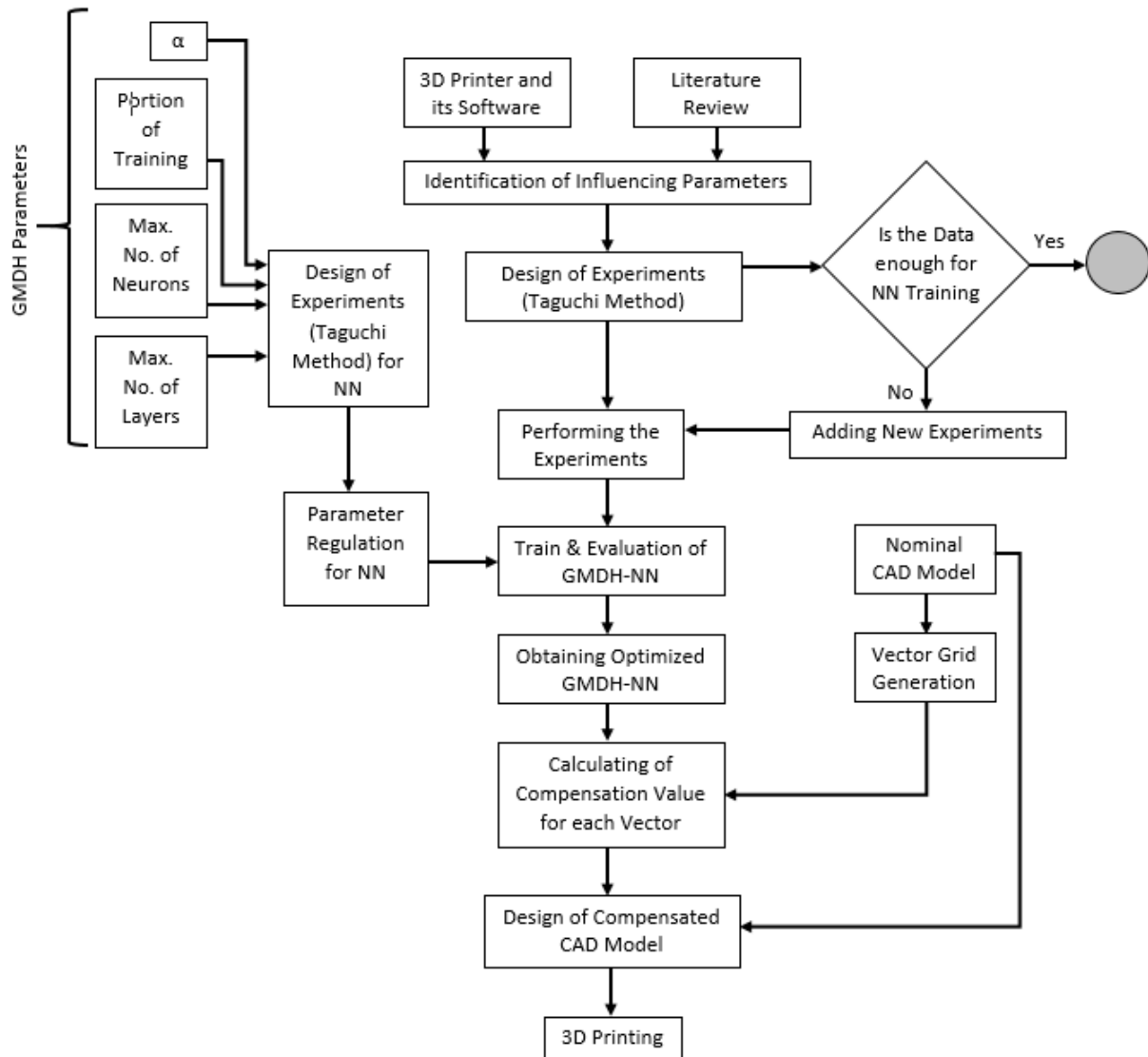


**Figure 5.** Flow-Chart of the proposed Method

## Results and Discussion:

As mentioned in Section 2.2, nine parameters, each with three levels, were identified after reviewing the research and investigating device settings and Makerbot Replicator 2X software. These are listed in Table 2. The test table for the Taguchi orthogonal arrays suggests a 27-test system in the L27 form for this study. For simplicity, categorical inputs are encoded as continuous, and later the results are decoded. As shown in Table 2, for Print location, the

numbers 1, 2, and 3 represent left, center, and right, respectively. The numbers 1, 2, and 3 represent the star, rectangular and hexagonal, sequentially for the infill pattern. To make the numbers as tangible as possible for infill density, the numbers 0.1, 0.2, and 0.3 represent 10%, 20%, and 30% infill, respectively. The input parameters are named x1 to x9 according to Table 2.

Hexagonal-shaped samples, which have four pairs of parallel faces with different angles, were used for this study. The height of the samples were 30 mm, and the distance of parallel faces was measured in three different heights of 10 mm, 20 mm, and 30 mm. Every sample was printed on a rectangle of 100 mm by 150 mm. Printing location was one of the process parameters, therefore, the hexagon was printed on three locations on the right, left or center of the rectangle. Part number was printed on the rectangle to prevent mistakes (See Figure 6).

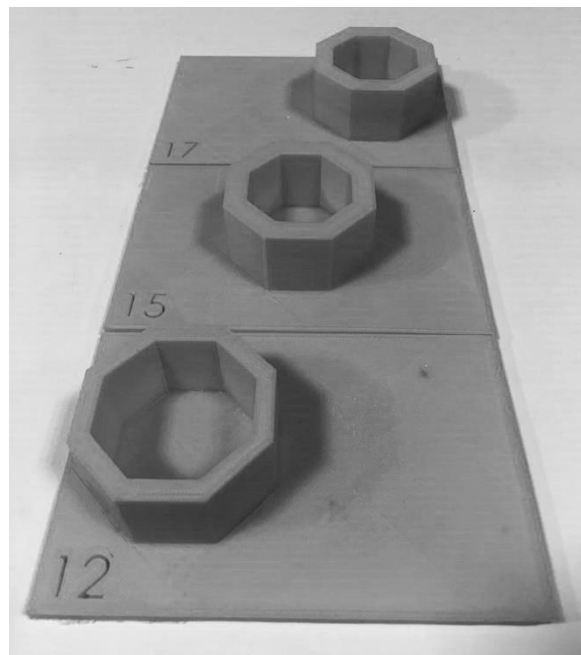


**Figure 6 .** The Hexagonal samples printed in different values of the input parameters

These 27 experiments give 27 pairs of data sets in the form of 9 inputs and one output. If a value is somewhat noisy or inaccurate, the probability of error increases in neural network training. Therefore, another 53 tests are randomly designed within the allowable range of parameters and added to the Taguchi list. Thus, there is a total of 80 tests. Parameter settings are done on the software, and a 3D printer creates the result. Material is ABS, and the measuring instrument is a micrometer with an accuracy of 0.001mm.

The Samples are measured by the three operators. The results of Taguchi-designed and randomly added experiments are shown in Tables 3 and 4, respectively. In these two tables, the nominal dimension represents the nominal CAD model's desired size, and the real dimension column represents the value measured on the printed model. The following formula produces the error value:

$$\text{Error} = \text{Nominal Dimension} - \text{Real Dimension}$$

The Taguchi tests' average error is 0.159 mm, and for the added points, the error is 0.153 mm, which indicates good compatibility.

**Table 3.** Results for Taguchi Tests

Order	X1	X2	X3	X4	X5	X6	X7	X8	X9	Nominal Dim	Real-Dim	Error
1	40	1	218	0	0.15	0.1	2	1	10	40	39.843	0.157
2	40	1	218	0	0.2	0.2	3	2	20	40	39.849	0.151
3	40	1	218	0	0.25	0.3	4	3	30	40	39.820	0.180
4	40	2	230	45	0.15	0.1	2	2	20	40	39.890	0.110
5	40	2	230	45	0.2	0.2	3	3	30	40	39.867	0.133
6	40	2	230	45	0.25	0.3	4	1	10	40	39.890	0.110
7	40	3	242	90	0.15	0.1	2	3	30	40	39.839	0.161
8	40	3	242	90	0.2	0.2	3	1	10	40	39.868	0.132
9	40	3	242	90	0.25	0.3	4	2	20	40	39.851	0.149
10	50	1	230	90	0.15	0.2	4	1	20	50	49.840	0.160
11	50	1	230	90	0.2	0.3	2	2	30	50	49.827	0.173
12	50	1	230	90	0.25	0.1	3	3	10	50	49.849	0.151
13	50	2	242	0	0.15	0.2	4	2	30	50	49.832	0.168
14	50	2	242	0	0.2	0.3	2	3	10	50	49.840	0.160
15	50	2	242	0	0.25	0.1	3	1	20	50	49.835	0.165
16	50	3	218	45	0.15	0.2	4	3	10	50	49.870	0.130
17	50	3	218	45	0.2	0.3	2	1	20	50	49.860	0.140
18	50	3	218	45	0.25	0.1	3	2	30	50	49.856	0.144
19	60	1	242	45	0.15	0.3	3	1	30	60	59.818	0.182
20	60	1	242	45	0.2	0.1	4	2	10	60	59.834	0.166
21	60	1	242	45	0.25	0.2	2	3	20	60	59.835	0.165
22	60	2	218	90	0.15	0.3	3	2	10	60	59.848	0.152
23	60	2	218	90	0.2	0.1	4	3	20	60	59.829	0.171
24	60	2	218	90	0.25	0.2	2	1	30	60	59.795	0.205
25	60	3	230	0	0.15	0.3	3	3	20	60	59.822	0.178
26	60	3	230	0	0.2	0.1	4	1	30	60	59.787	0.213
27	60	3	230	0	0.25	0.2	2	2	10	60	59.825	0.175
Average												0.159

**Table 4.** Results for Additional Tests

Order	X1	X2	X3	X4	X5	X6	X7	X8	X9	Nominal Dim	Real-Dim	Err
28	55	1	239	18	0.21	0.29	5	3	20	55	54.836	0.164
29	56	1	241	60	0.13	0.22	5	3	33	56	55.851	0.149
30	55	1	217	42	0.13	0.14	3	2	40	55	54.837	0.163
31	46	2	243	15	0.26	0.13	5	2	40	46	45.836	0.164
32	56	3	216	19	0.16	0.12	4	3	21	56	55.836	0.164
33	43	2	240	61	0.13	0.18	4	2	40	43	42.847	0.153
34	46	3	227	13	0.12	0.25	3	2	20	46	45.883	0.117
35	46	1	229	89	0.18	0.29	2	3	33	46	45.844	0.156
36	58	2	219	41	0.24	0.12	2	1	38	58	57.812	0.188
37	51	3	227	80	0.21	0.28	2	1	32	51	50.835	0.165
38	48	1	227	29	0.18	0.14	2	2	28	48	47.879	0.121
39	44	3	217	19	0.21	0.26	2	3	23	44	43.861	0.139
40	42	3	224	71	0.3	0.24	3	1	19	42	41.864	0.136
41	51	1	224	54	0.14	0.14	4	2	27	51	50.875	0.125
42	60	2	225	47	0.28	0.3	5	2	33	60	59.817	0.183
43	59	3	230	26	0.22	0.17	5	2	39	59	58.821	0.179
44	54	3	244	85	0.27	0.14	5	2	19	54	53.837	0.163
45	51	3	232	24	0.18	0.14	3	1	36	51	50.835	0.165
46	48	1	225	76	0.16	0.26	4	1	26	48	47.844	0.156
47	46	3	238	41	0.14	0.13	3	2	35	46	45.875	0.125
48	54	1	220	23	0.24	0.12	3	3	38	54	53.828	0.172
49	52	3	238	63	0.24	0.16	4	2	35	52	51.817	0.183
50	41	1	245	74	0.23	0.24	5	1	30	41	40.841	0.159
51	41	2	231	79	0.14	0.29	5	1	29	41	40.856	0.144
52	51	2	226	31	0.12	0.18	2	2	32	51	50.871	0.129
53	43	3	243	75	0.2	0.24	3	2	12	43	42.860	0.140
54	59	1	230	35	0.21	0.3	5	1	34	59	58.848	0.152

55	50	2	240	79	0.3	0.14	5	1	23	50	49.823	0.177
56	57	2	228	9	0.24	0.25	3	2	33	57	56.802	0.198
57	60	3	218	43	0.23	0.21	2	1	40	60	59.819	0.181
58	56	3	226	19	0.24	0.18	3	3	36	56	55.826	0.174
59	48	3	224	27	0.16	0.11	5	3	18	48	47.867	0.133
60	50	3	227	20	0.25	0.26	4	2	33	50	49.847	0.153
61	51	1	216	53	0.14	0.14	2	2	11	51	50.885	0.115
62	50	1	229	15	0.22	0.27	2	1	18	50	49.849	0.151
63	48	2	219	37	0.24	0.21	3	2	31	48	47.853	0.147
64	43	2	244	52	0.22	0.26	2	3	19	43	42.872	0.128
65	52	2	227	23	0.29	0.19	4	2	31	52	51.859	0.141
66	49	1	236	84	0.18	0.23	5	2	29	49	48.849	0.151
67	50	1	219	10	0.19	0.29	4	3	12	50	49.863	0.137
68	47	3	216	16	0.26	0.27	4	2	39	47	46.818	0.182
69	55	3	238	79	0.3	0.3	5	1	12	55	54.828	0.172
70	57	1	217	70	0.21	0.17	4	3	30	57	56.838	0.162
71	49	2	221	22	0.15	0.16	5	2	35	49	48.858	0.142
72	48	1	238	79	0.18	0.14	5	3	15	48	47.850	0.150
73	59	2	222	13	0.16	0.21	2	2	11	59	58.853	0.147
74	50	1	244	28	0.19	0.24	3	1	13	50	49.861	0.139
75	47	3	234	19	0.3	0.19	5	2	11	47	46.874	0.126
76	41	3	229	26	0.28	0.24	3	2	18	41	40.884	0.116
77	44	2	232	84	0.25	0.13	2	1	38	44	43.841	0.159
78	54	1	244	11	0.2	0.18	3	1	20	54	53.824	0.176
79	46	1	244	3	0.29	0.18	4	3	13	46	45.838	0.162
80	54	2	219	45	0.2	0.28	4	1	30	54	53.855	0.145
Average												0.153

We used Minitab 19 software to analyze the results. The ANOVA analysis results are listed in Table 5, and the Main effect plots for S / N ratios are presented in Figure 7. In this analysis, the "smaller is better" strategy is taken due to the nature of the output (error).

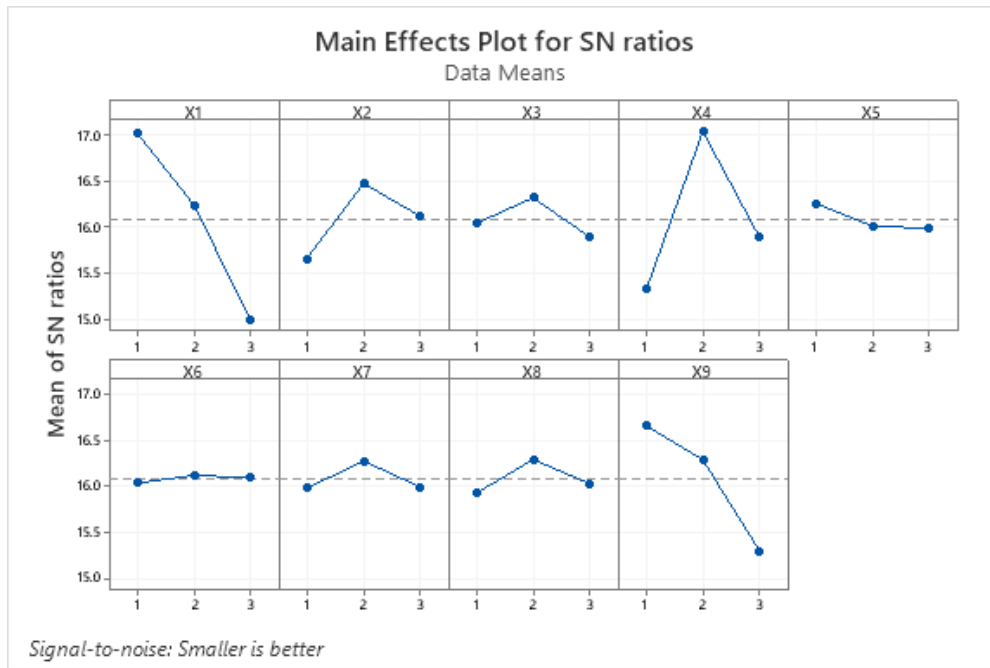


**Figure 7.** 3D Printed Parts: Main Effects Plot for S/N Ratios (Smaller is Better)

**Table 5.** 3D Printed Parts: Response Table for Signal to Noise Ratios (Smaller is better)

Level	X1	X2	X3	X4	X5	X6	X7	X8	X9
1	17.02	15.66	16.05	15.33	16.26	16.04	15.99	15.93	16.66
2	16.25	16.48	16.32	17.04	16.02	16.13	16.28	16.30	16.30
3	15.00	16.12	15.90	15.90	15.99	16.10	16.00	16.04	15.31
Delta	2.03	0.82	0.43	1.71	0.27	0.08	0.29	0.36	1.36
Rank	1	4	5	2	8	9	7	6	3

Figure 7 and Table 5 show that the most influential factor is the scale, and the least effective factor is infill density. According to ANOVA analysis, scale and infill density have a Delta value of 2.03 and 0.08, respectively. The ratio of the least effective to the most effective factor is 0.0394, or about 4%. Therefore, all factors remain in the neural network training. Figure 7 also shows that the optimal position for "scale" is 40 mm. For the print location, the optimal state happens when the sample position is in the middle of the printer desk. The best extruder temperature for ABS filament happens at 230° C. In the 45° orientation the error is minimum. The figure also shows that the number of shells should be three, and their pattern type should be rectangular for optimum state. Moreover, lower heights are shown to cause a smaller error. The smaller the Layer thickness factor is, the better. The model's density does not significantly affect the output error, although the 20% density parts have slightly less error than 10% and 30% density parts. The results from Tables 3 and 4 are then integrated and given as input data to the GMDH neural network with the following initial settings:

P-train: 0.8 (80%)

Number of layers: 3

Number of neurons: 6

$\alpha = 0.7$

The calculated RSME of 0.0107 and the R-value of 0.869 indicate the relative proportionality of the results. Therefore, four variables with three levels are selected as the neural network configuration variables according to Table 6. Note that these levels are not mandatory and are entirely determined by the user. The Taguchi L9 orthogonal array table determines the test settings.

**Table 6.** Input parameters with their levels for GMDH-NN Performance Optimization

No.	Variable Name	Level 1	Level 2	Level 3
1	Max. No. of Neurons	3	6	9
2	Max. No. of Layers	3	5	7
3	Alpha	0.5	0.7	0.9
4	P-Train	0.6	0.7	0.8

Available data obtained from Taguchi designed experiments combined with random points were fed to the GMDH network, each time with one of the proposed settings. The RSME values and the R-values are measured for all data, then listed in Table 7. Moreover, the main effects plot for S/N ratios is shown in Figure 8. Due to the nature of the RSME output, the smaller is better strategy is used in this analysis. Table 8 shows the results of the ANOVA analysis for the regulation of GMDH neural network input parameters. According to these results, the optimal value are as follows:

Maximum number of Neurons = 6

Maximum number of layers = 3

$\alpha = 0.5$

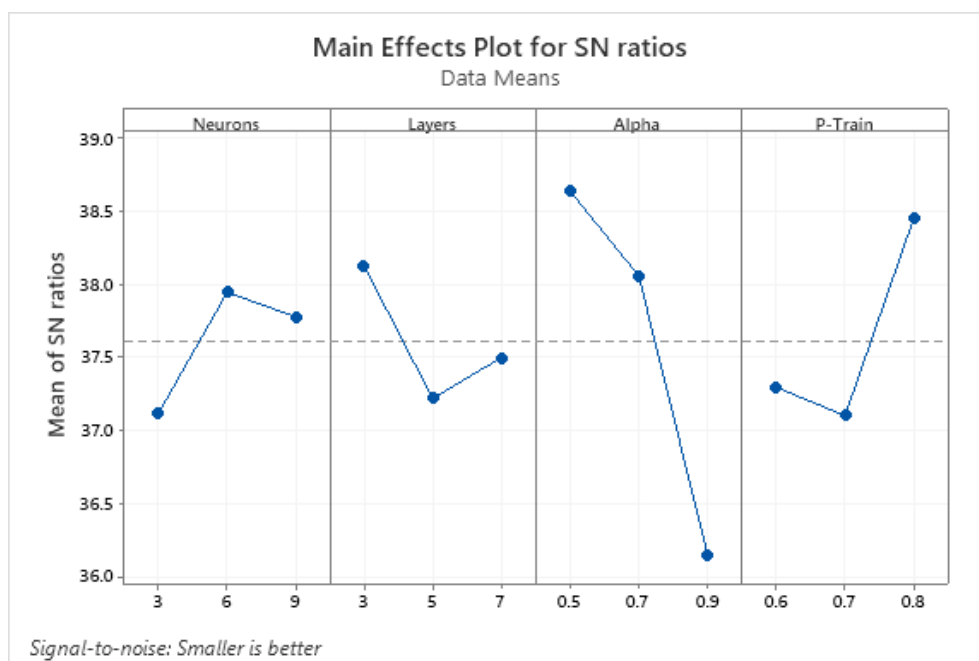
P-train = 0.8 (or 80%)

**Table 7.** GMDH-NN: Results for Taguchi L<sub>9</sub> Tests

No.	Max. No. of Neurons	Max. No. of Layers	Alpha	P-Train	RSME	R
1	3	3	0.5	0.6	0.0121	0.827
2	3	5	0.7	0.7	0.0147	0.754
3	3	7	0.9	0.8	0.0152	0.719
4	6	3	0.7	0.8	0.0107	0.869
5	6	5	0.9	0.6	0.0163	0.696
6	6	7	0.5	0.7	0.0121	0.83
7	9	3	0.9	0.7	0.0153	0.707
8	9	5	0.5	0.8	0.0109	0.863
9	9	7	0.7	0.6	0.0129	0.823

**Table 8.** GMDH-NN Performance: Response Table for Signal to Noise Ratios (Smaller is better)

Level	Neurons	Layers	Alpha	P-Train
1	37.12	38.13	38.65	37.30
2	37.95	37.22	38.06	37.10
3	37.78	37.50	36.14	38.45
Delta	0.83	0.91	2.50	1.35
Rank	4	3	1	2

**Figure 8.** GMDH-NN Performance: Main Effects Plot for S/N Ratios (Smaller is Better)

In this case, RSME is 0.0103, and R-value is 0.878. The performance curves of the GMDH neural network training in the optimal state are presented in Figure 9. The diagrams in Figure 10 show the difference between the Nominal CAD model and the one predicted by the prepared model for each of the 80 input data sets. The relatively good fitting and the RSME value of 0.0103 show the high quality of the created mathematical model. Furthermore, the average error of -0.001, knowing that its ideal state is zero and the standard deviation of 0.0103, is very close to the model's RSME value. This shows the appropriate distribution of error and confirms the optimal performance of the mathematical model.

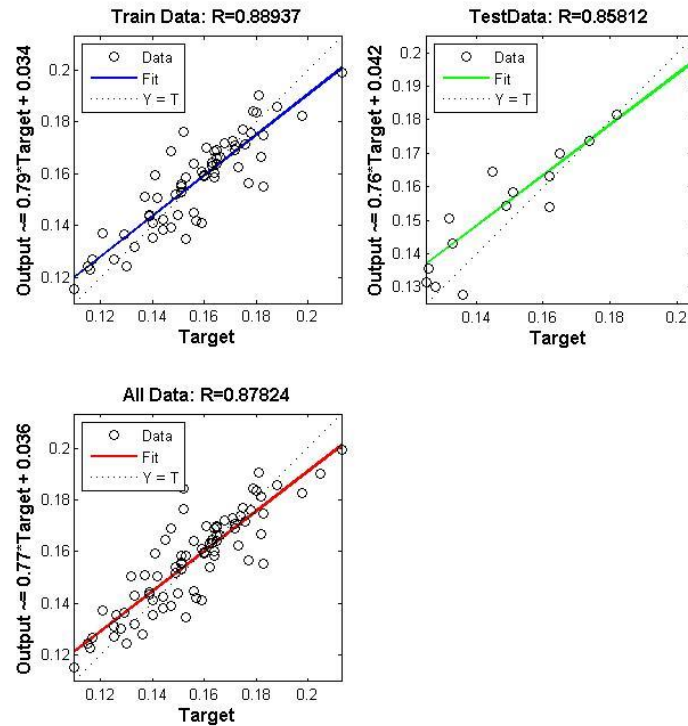


**Figure 9.** GMDH-NN: Training Performance

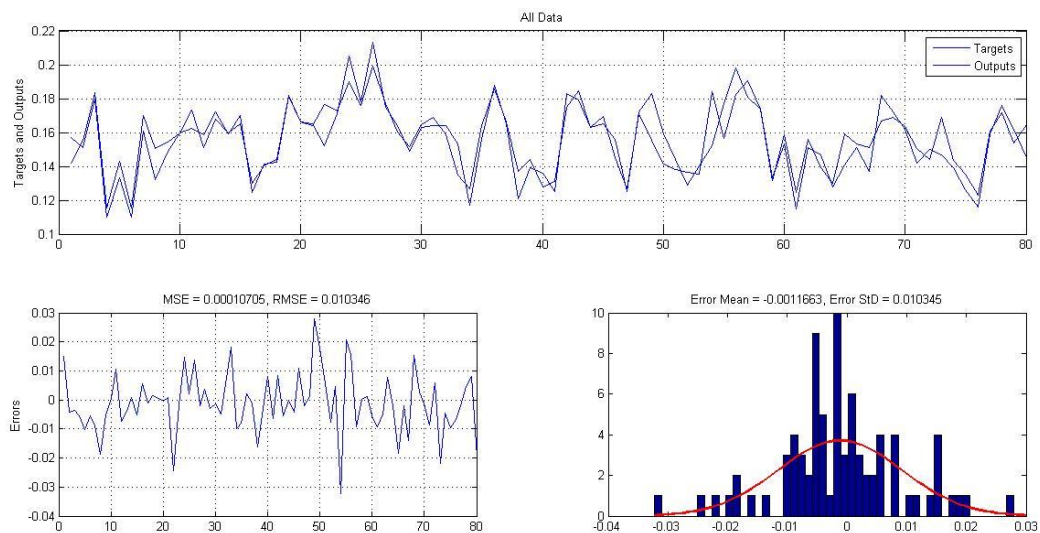


**Figure 10.** GMDH-NN: The difference between Predicted Model Error (Output) & Real Error (Target)

## Case study

Assume the given Nominal CAD model is as shown in Figure 11. We create a compensated curve for the free form edge of the body by placing the coordinates' origin on the two perpendicular lines' intersection point.

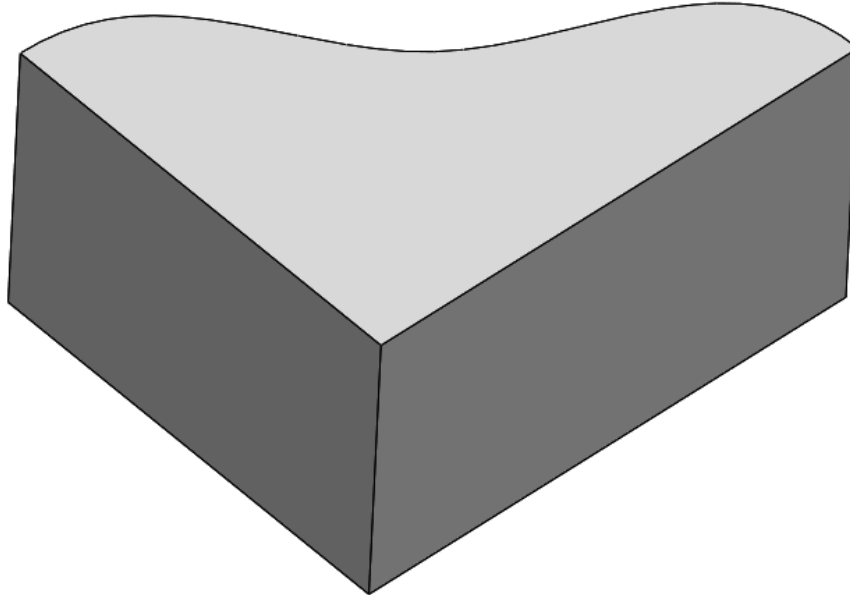


**Figure 11.** Nominal CAD Model for case study

For this purpose, we select the points P0 to P6 on the curve as shown in Figure 12 and report their  $x$ ,  $y$ ,  $R$ , and  $\theta$  values in Table 9. According to section 2.2, we choose the factor  $x_1$  is the length of each point's vector. Similarly, the  $x_4$  factor is chosen to be the angle of each point's vector. Also, the factor  $x_9$  is selected as the height of the points, which in this model are 15 mm for all points. Other parameters are set to their optimal values and are equal for all selected points. They are constant during the test. This arrangement is shown in Table 10. The above values are given to the optimized GMDH neural network, and the output is taken. This output is  $R_{c_i} = -e_i$ , where  $e_i$  is the error between the nominal CAD model and the actual printed model. The values obtained for  $R_{c_i}$  are listed in Table 11. With respect to these values,  $R_i$  at any point is converted to  $(R_i + R_{c_i})$ , and is called R-compensated.

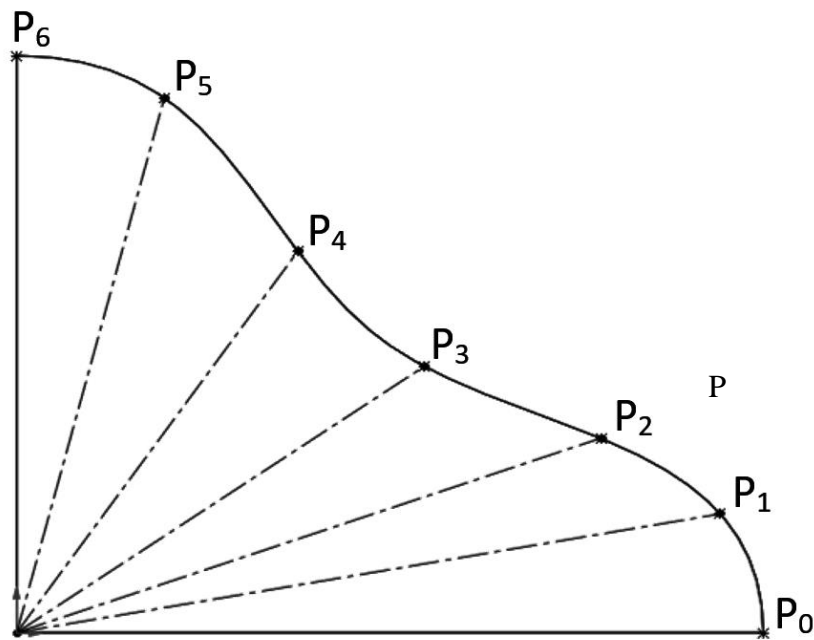


**Figure 12.** Selection of Indicator points and polar vectors

**Table 9.** Selected points for generating the compensation Model

Point	X	Y	R	$\theta$
P0	60.00	0.00	60.00	0.00
P1	56.55	10.29	57.48	10.31
P2	46.93	16.84	49.86	19.74
P3	32.76	23.07	40.07	35.15
P4	22.59	33.05	40.03	55.65
P5	11.86	46.35	47.84	75.65
P6	0.00	50.00	50.00	90.00

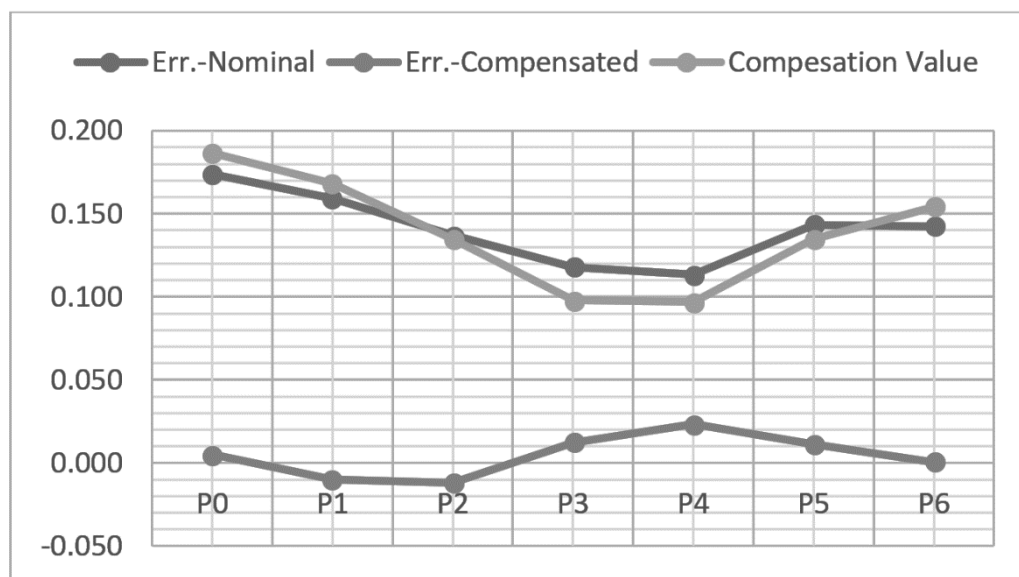
**Table 10.** Input values for selected points in the case study

Point	X1	X2	X3	X4	X5	X6	X7	X8	X9
P0	60	2	230	0	0.15	50	3	2	15
P1	57.479	2	230	10.31	0.15	50	3	2	15
P2	49.86	2	230	19.74	0.15	50	3	2	15
P3	40.068	2	230	35.15	0.15	50	3	2	15
P4	40.033	2	230	55.65	0.15	50	3	2	15
P5	47.843	2	230	75.65	0.15	50	3	2	15
P6	50	2	230	90	0.15	50	3	2	15

**Table 11.** Predicted Compensation values for selected points

Point	Compensation Value
P0	0.186
P1	0.168
P2	0.135
P3	0.098
P4	0.097
P5	0.135
P6	0.154

3D printing is done once using the Nominal CAD model and once using the compensated CAD model to evaluate the extent of the effects of compensation. Printed radius values are recorded in the columns of Table 12 under the headings Real-R-Nominal and Real-R-Compensated, respectively. Also, we put the error measure of each in the Err-Nominal and Err-compensated` columns, respectively. According to Table 12, the RSME value of the nominal model without compensation is 0.377. After implementing the compensation, this value is 0.033. This can be seen in Figure 13. The proximity of the true  $-e_i$  diagrams in the nominal state to the value of  $R_{ci}$  predicted by the mathematical model and the neural network indicates the correct performance of the prediction. Also, the compensated model error diagram in Figure 13 fluctuates around 0, which confirms the correct operation of Model 1.

**Figure 13.** Comparison between Nominal Error, Compensated Error and Compensation Value

**Table 12.** Results for 3D Printed Part using Nominal and Compensated CAD Model

Point	R-Nominal	R-Compensated	R-Real-Nominal	Err.-Nominal	R-Real-Compensated	Err.-Compensated
P0	60.000	60.186	59.826	0.174	59.995	0.005
P1	57.479	57.647	57.320	0.159	57.489	-0.010
P2	49.860	49.995	49.723	0.137	49.872	-0.012
P3	40.068	40.166	39.950	0.118	40.056	0.012
P4	40.033	40.130	39.920	0.113	40.010	0.023
P5	47.843	47.978	47.700	0.143	47.832	0.011
P6	50.000	50.154	49.858	0.142	49.999	0.001
RSME				0.377		0.033

### Limitations and future work

The most important limitations of the research are the small number of samples due to the expensive sampling process, as well as its time consuming. On the other hand, the impossibility of accurate measurements due to the wall roughness (generally in the FDM process) can affect the results. Future research could be to do this research with more data, as well as repeat sampling for each record, in order to cover possible errors and measurements in a automatic way and with more accurate tools.

### Conclusion

In this research, an error compensation model is presented regardless of the error sources. In this model's development, the elimination of disturbance (which may happen because of inadequate and noisy data) in the results and the model's comprehensiveness in terms of input parameters have been considered.

Nine parameters are identified and then experiments are designed using Taguchi orthogonal arrays, L27 with 3 levels for each parameter. To compensate for the small number of existing multi-input–single-output sets, another 53 experiments were randomly selected by adjusting the inputs within their allowable range. Hence a total of 80 experiments are conducted, and the results are recorded.

The results are fed to a GMDH neural network, which is capable for limited or noisy data sets, where the regulatory parameters of the network are optimized. The output is considered a mathematical model of the process.

Finally, a case study is performed on the results. After implementing the above algorithm and performing the compensation, the error rate is reduced from 0.377 to 0.33, as shown in Figure 13. The proximity of the error curves in the actual nominated state and the amount of compensation offered by this compensator indicates its accurate execution. Also, the fluctuation of error around zero confirms the correct performance of the compensator.

## References

- [1] S. O. Onuh, Y. Y. Yusuf, Rapid prototyping technology: applications and benefits for rapid product development, *Journal of intelligent manufacturing*, Vol. 10, No. 3, pp. 301-311, 1999.
- [2] C. Lee, S. Kim, H. Kim, S.-H. Ahn, Measurement of anisotropic compressive strength of rapid prototyping parts, *Journal of materials processing technology*, Vol. 187, pp. 627-630, 2007.
- [3] J.-P. Kruth, M.-C. Leu, T. Nakagawa, Progress in additive manufacturing and rapid prototyping, *Cirp Annals*, Vol. 47, No. 2, pp. 525-540, 1998.
- [4] B. H. Lee, J. Abdullah, Z. A. Khan, Optimization of rapid prototyping parameters for production of flexible ABS object, *Journal of materials processing technology*, Vol. 169, No. 1, pp. 54-61, 2005.
- [5] B. N. Turner, R. Strong, S. A. Gold, A review of melt extrusion additive manufacturing processes: I. Process design and modeling, *Rapid Prototyping Journal*, 2014.
- [6] A. Sood, R. Ohdar, S. Mahapatra, Parametric appraisal of fused deposition modelling process using the grey Taguchi method, *Proceedings of the Institution of Mechanical Engineers, Part B: Journal of Engineering Manufacture*, Vol. 224, No. 1, pp. 135-145, 2010.
- [7] L. Villalpando, H. Eiliat, R. J. Urbanic, An optimization approach for components built by fused deposition modeling with parametric internal structures, *Procedia Cirp*, Vol. 17, pp. 800-805, 2014.
- [8] I. El-Katatny, S. Masood, Y. Morsi, Error analysis of FDM fabricated medical replicas, *Rapid Prototyping Journal*, 2010.
- [9] G. Percoco, L. Galantucci, F. Lavecchia, Validation study of an analytical model of FDM accuracy, *DAAAM International Scientific Book, Published by DAAAM International Vienna, Austria*, pp. 585-592, 2011.
- [10] O. A. Mohamed, S. H. Masood, J. L. Bhowmik, Modeling, analysis, and optimization of dimensional accuracy of FDM-fabricated parts using definitive screening design and deep learning feedforward artificial neural network, *Advances in Manufacturing*, Vol. 9, No. 1, pp. 115-129, 2021.
- [11] O. E. Akbaş, O. Hira, S. Z. Hervean, S. Samankan, A. Altınkaynak, Dimensional accuracy of FDM-printed polymer parts, *Rapid Prototyping Journal*, 2019.
- [12] J.-M. Park, J. Jeon, J.-Y. Koak, S.-K. Kim, S.-J. Heo, Dimensional accuracy and surface characteristics of 3D-printed dental casts, *The Journal of prosthetic dentistry*, 2020.
- [13] A. Peng, X. Xiao, R. Yue, Process parameter optimization for fused deposition modeling using response surface methodology combined with fuzzy inference system, *The International Journal of Advanced Manufacturing Technology*, Vol. 73, No. 1-4, pp. 87-100, 2014.
- [14] R. Mendricky, D. Fris, Analysis of the Accuracy and the Surface Roughness of FDM/FFF Technology and Optimisation of Process Parameters, *Tehnički vjesnik*, Vol. 27, No. 4, pp. 1166-1173, 2020.
- [15] J. S. Chohan, R. Singh, K. S. Boparai, R. Penna, F. Fraternali, Dimensional accuracy analysis of coupled fused deposition modeling and vapour smoothing operations for biomedical applications, *Composites Part B: Engineering*, Vol. 117, pp. 138-149, 2017.
- [16] A. Garg, A. Bhattacharya, A. Batish, On surface finish and dimensional accuracy of FDM parts after cold vapor treatment, *Materials and Manufacturing Processes*, Vol. 31, No. 4, pp. 522-529, 2016.
- [17] J. Nsengimana, J. Van der Walt, E. Pei, M. Miah, Effect of post-processing on the dimensional accuracy of small plastic additive manufactured parts, *Rapid Prototyping Journal*, 2019.
- [18] P. K. Garg, R. Singh, I. Ahuja, Multi-objective optimization of dimensional accuracy, surface roughness and hardness of hybrid investment cast components, *Rapid Prototyping Journal*, 2017.
- [19] K. Tong, S. Joshi, E. A. Lehtihet, Error compensation for fused deposition modeling (FDM) machine by correcting slice files, *Rapid Prototyping Journal*, 2008.
- [20] S. Li, T. Liu, X. Xiao, W. Hu, W. Liao, Study on Size Error Compensation of Connecting Bracket Based on Fused Deposition Modeling, in *Proceeding of*, IOP Publishing, pp. 012013.
- [21] R. Păcurar, V. Buzilă, A. Păcurar, E. Guțiu, S. D. Stan, P. Berce, Research on improving the accuracy of FDM 3D printing process by using a new designed calibrating part, in *Proceeding of*, EDP Sciences, pp. 01007.
- [22] U. Yaman, Shrinkage compensation of holes via shrinkage of interior structure in FDM process, *The International Journal of Advanced Manufacturing Technology*, Vol. 94, No. 5, pp. 2187-2197, 2018.
- [23] U. M. Dilberoglu, S. Simsek, U. Yaman, Shrinkage compensation approach proposed for ABS material in FDM process, *Materials and Manufacturing Processes*, Vol. 34, No. 9, pp. 993-998, 2019.
- [24] A. Noriega, D. Blanco, B. Alvarez, A. Garcia, Dimensional accuracy improvement of FDM square cross-section parts using artificial neural networks and an optimization algorithm, *The International Journal of Advanced Manufacturing Technology*, Vol. 69, No. 9-12, pp. 2301-2313, 2013.
- [25] D. A. Bircan, *Development of a NURBS based adaptive slicing procedure for fused deposition modeling in rapid prototyping applications*, Thesis, PhD thesis, Cukurova University, 2008.

- [26] F. Górski, W. Kuczko, R. Wichniarek, Influence of process parameters on dimensional accuracy of parts manufactured using Fused Deposition Modelling technology, *Advances in Science and Technology Research Journal*, Vol. 7, No. 19, pp. 27--35, 2013.
- [27] F. Rayegani, G. C. Onwubolu, Fused deposition modelling (FDM) process parameter prediction and optimization using group method for data handling (GMDH) and differential evolution (DE), *The International Journal of Advanced Manufacturing Technology*, Vol. 73, No. 1-4, pp. 509-519, 2014.
- [28] A. K. Sood, R. Ohdar, S. S. Mahapatra, Improving dimensional accuracy of fused deposition modelling processed part using grey Taguchi method, *Materials & Design*, Vol. 30, No. 10, pp. 4243-4252, 2009.
- [29] S. K. Panda, S. Padhee, S. Anoop Kumar, S. S. Mahapatra, Optimization of fused deposition modelling (FDM) process parameters using bacterial foraging technique, *Intelligent information management*, Vol. 1, No. 02, pp. 89, 2009.
- [30] A. Arivazhagan, S. Masood, Dynamic mechanical properties of ABS material processed by fused deposition modelling, *Int. J. Eng. Res. Appl*, Vol. 2, No. 3, pp. 2009-2014, 2012.
- [31] O. Luzanin, D. Movrin, M. Plancak, EXPERIMENTAL INVESTIGATION OF EXTRUSION SPEED AND TEMPERATURE EFFECTS ON ARITHMETIC MEAN, *Journal for Technology of Plasticity*, Vol. 38, No. 2, 2013.
- [32] R. K. Sahu, S. Mahapatra, A. K. Sood, A study on dimensional accuracy of fused deposition modeling (FDM) processed parts using fuzzy logic, *Journal for Manufacturing Science and Production*, Vol. 13, No. 3, pp. 183, 2013.
- [33] S. Bhatia, *Effect of machine positional errors on geometric tolerances in additive manufacturing*, Thesis, University of Cincinnati, 2014.
- [34] S. O. Akande, Dimensional accuracy and surface finish optimization of fused deposition modelling parts using desirability function analysis, *International Journal of Engineering Research and Technology*, Vol. 4, No. 4, pp. 196-202, 2015.
- [35] L. Baich, G. Manogharan, H. Marie, Study of infill print design on production cost-time of 3D printed ABS parts, *International Journal of Rapid Manufacturing*, Vol. 5, No. 3-4, pp. 308-319, 2015.
- [36] A. Equbal, A. K. Sood, A. Ansari, A. Equbal, Optimization of process parameters of FDM part for minimizing its dimensional inaccuracy, *International Journal of Mechanical and Production Engineering Research and Development*, Vol. 7, No. 2, pp. 57-65, 2017.
- [37] R. Narang, D. Chhabra, Analysis of process parameters of fused deposition modeling (FDM) technique, *International Journal on Future Revolution in Computer Science & Communication Engineering*, Vol. 3, No. 10, pp. 41-48, 2017.
- [38] A. Qattawi, B. Alrawi, A. Guzman, Experimental optimization of fused deposition modelling processing parameters: a design-for-manufacturing approach, *Procedia Manufacturing*, Vol. 10, pp. 791-803, 2017.
- [39] Y. Y. Aw, C. K. Yeoh, M. A. Idris, P. L. Teh, K. A. Hamzah, S. A. Sazali, Effect of printing parameters on tensile, dynamic mechanical, and thermoelectric properties of FDM 3D printed CABS/ZnO composites, *Materials*, Vol. 11, No. 4, pp. 466, 2018.
- [40] X. Deng, Z. Zeng, B. Peng, S. Yan, W. Ke, Mechanical properties optimization of poly-ether-ether-ketone via fused deposition modeling, *Materials*, Vol. 11, No. 2, pp. 216, 2018.
- [41] M. Leite, J. Fernandes, A. M. Deus, L. Reis, M. F. Vaz, Study of the influence of 3D printing parameters on the mechanical properties of PLA, in *Proceeding of*.
- [42] A. Dey, N. Yodo, A systematic survey of FDM process parameter optimization and their influence on part characteristics, *Journal of Manufacturing and Materials Processing*, Vol. 3, No. 3, pp. 64, 2019.
- [43] J. Lyu, S. Manoochchri, Error modeling and compensation for FDM machines, *Rapid Prototyping Journal*, 2019.
- [44] L. Natrayan, M. S. Kumar, An integrated artificial neural network and Taguchi approach to optimize the squeeze cast process parameters of AA6061/Al<sub>2</sub>O<sub>3</sub>/SiC/Gr hybrid composites prepared by novel encapsulation feeding technique, *Materials Today Communications*, Vol. 25, pp. 101586, 2020.
- [45] F. Halladj, A. Boukhiar, H. Amellal, S. Benamara, Optimization of traditional date vinegar preparation using full factorial design, *Journal of the American Society of Brewing Chemists*, Vol. 74, No. 2, pp. 137-144, 2016.
- [46] S. Ree, Y. H. Park, H. Yoo, A study on education quality using the Taguchi method, *Total Quality Management & Business Excellence*, Vol. 25, No. 7-8, pp. 935-943, 2014.
- [47] H. Rangaswamy, I. Sogalad, S. Basavarajappa, S. Acharya, G. Manjunath Patel, Experimental analysis and prediction of strength of adhesive-bonded single-lap composite joints: Taguchi and artificial neural network approaches, *SN Applied Sciences*, Vol. 2, pp. 1-15, 2020.
- [48] C. Camposeco-Negrete, Optimization of FDM parameters for improving part quality, productivity and sustainability of the process using Taguchi methodology and desirability approach, *Progress in Additive Manufacturing*, Vol. 5, No. 1, pp. 59-65, 2020.

- [49] K. Elbaz, S.-L. Shen, A. Zhou, Z.-Y. Yin, H.-M. Lyu, Prediction of Disc Cutter Life during Shield Tunneling with AI via the Incorporation of a Genetic Algorithm into a GMDH-Type Neural Network, *Engineering*, 2020.
- [50] L. Anastasakis, N. Mort, The development of self-organization techniques in modelling: a review of the group method of data handling (GMDH), *RESEARCH REPORT-UNIVERSITY OF SHEFFIELD DEPARTMENT OF AUTOMATIC CONTROL AND SYSTEMS ENGINEERING*, 2001.
- [51] M. H. Ahmadi, M. Sadeghzadeh, A. H. Raffiee, K.-w. Chau, Applying GMDH neural network to estimate the thermal resistance and thermal conductivity of pulsating heat pipes, *Engineering Applications of Computational Fluid Mechanics*, Vol. 13, No. 1, pp. 327-336, 2019.
- [52] M. Bildirici, Ö. Ersin, Modeling Markov switching ARMA-GARCH neural networks models and an application to forecasting stock returns, *The Scientific World Journal*, Vol. 2014, 2014.
- [53] H. Elçiçek, E. Akdoğan, S. Karagöz, The use of artificial neural network for prediction of dissolution kinetics, *The Scientific World Journal*, Vol. 2014, 2014.
- [54] A. Gonzalez-Sanchez, J. Frausto-Solis, W. Ojeda-Bustamante, Attribute selection impact on linear and nonlinear regression models for crop yield prediction, *The Scientific World Journal*, Vol. 2014, 2014.
- [55] D. J. Armaghani, M. Hasanipanah, H. B. Amnieh, D. T. Bui, P. Mehrabi, M. Khorami, Development of a novel hybrid intelligent model for solving engineering problems using GS-GMDH algorithm, *Engineering with Computers*, pp. 1-13, 2019.
- [56] D. Li, D. J. Armaghani, J. Zhou, S. H. Lai, M. Hasanipanah, A GMDH predictive model to predict rock material strength using three non-destructive tests, *Journal of Nondestructive Evaluation*, Vol. 39, No. 4, pp. 1-14, 2020.
- [57] M. Dorn, A. L. Braga, C. H. Llanos, L. S. Coelho, A GMDH polynomial neural network-based method to predict approximate three-dimensional structures of polypeptides, *Expert Systems with Applications*, Vol. 39, No. 15, pp. 12268-12279, 2012.